Solid-state synthesis and characterization of ferromagnetic Mn_5Ge_3 nanoclusters in GeO/Mn thin films

V. G. Myagkov [a], A. A. Matsynin [a], L. E. Bykova [a], V. S. Zhigalov [a], Yu. L. Mikhlin [b], M. N. Volochaev [a,c], D. A. Velikanov [a], A. S. Aleksandrovsky [a,d], G. N. Bondarenko [b]

[a] Kirensky Institute of Physics, Federal Research Center KSC SB RAS, Russian Academy of Sciences, Krasnoyarsk, 660036, Russia
[b] Institute of Chemistry and Chemical Technology, Federal Research Center KSC SB RAS, Russian Academy of Sciences, Krasnoyarsk, 660036, Russia
[c] Siberian State Aerospace University, Krasnoyarsk, 660014, Russia
[d] Institute of Nanotechnology, Spectroscopy and Quantum Chemistry, Siberian Federal University, Krasnoyarsk 660041, Russia

Keywords: Mn-Ge system, Thin-film solid-state reactions, Mn_5Ge_3 alloy, Nowotny $Mn_5Ge_3O_y$ phase, magnetic properties.

Abstract

Mn_5Ge_3 films are promising materials for spintronic applications due to their high spin polarization and a Curie temperature above room temperature. However, non-magnetic elements such as oxygen, carbon and nitrogen may unpredictably change the structural and magnetic properties of Mn_5Ge_3 films. Here, we use the solid-state reaction between Mn and GeO thin films to describe the synthesis and the structural and magnetic characterization of $Mn_5Ge_3(Mn_5Ge_3O_y)$-$GeO_2(GeO_x)$ nanocomposite materials. Our results show that the synthesis of these nanocomposites starts at 180°C when the GeO decomposes into elemental germanium and oxygen and the resulting Ge atoms immediately migrate into the Mn layer to form ferromagnetic Mn_5Ge_3 nanoclusters. At the same time the oxygen atoms take part in the synthesis of GeO_x and GeO_2 oxides and also migrate into the Mn_5Ge_3 lattice to form $Mn_5Ge_3O_y$ Nowotny nanoclusters. Our findings prove that not only carbon, but oxygen may contribute to the increase of the magnetization saturation and Curie temperature of Mn_5Ge_3-based nanostructures.

Introduction

In recent years, the synthesis features and structural, electronic and magnetic properties of ferromagnetic Mn_5Ge_3 films have been intensively studied for future applications in spintronics [1-5]. An important advantage of Mn_5Ge_3 is a sufficiently high spin polarization [6, 7] and epitaxial growth on Ge (111) and Ge (001) substrates by solid-phase epitaxy [8-11]. Thus, in epitaxial Mn_5Ge_3/Ge (111) and Mn_5Ge_3/Ge (001) samples, the ferromagnetic Mn_5Ge_3 compound can potentially be used as a source of spin injection into the Ge layer [8-11]. However, Mn_5Ge_3 has a Curie temperature only slightly above room temperature (T_C = 304 K) and a higher T_C is required for technological applications. A common method of increasing the Curie temperature is doping with Mn_5Ge_3 samples [8,9,12,13]. For epitaxial $Mn_5Ge_3C_x$ films the Curie temperature increases with the carbon concentration and reaches a maximum T_C = 460K at x ~ 0.6 - 0.7 [13]. The homogeneous distribution of oxygen and carbon in Mn_5Ge_3 films obtained in a vacuum of 10^{-6} mbar suggests that the increase in the Curie temperature and magnetization is due to the migration of gas C and O impurities to the Mn_5Ge_3 lattice and the formation of the Novotny phase of $Mn_5Ge_3C_xO_y$ [14-16]. Experimental studies have shown that N, C and O impurities, which are present even in ultra-high vacuum, are embedded in the Mn_5Ge_3 lattice during precipitation or annealing and increase the magnetic and electrical properties [17-20]. Calculations show, as a result of the reactivity of manganese, that at high oxygen concentrations the structural and magnetic properties of Mn-

doped germanium are greatly reduced or even suppressed [21]. However, the effect of oxygen on the chemical interaction of Mn with Ge is still poorly understood.

Herein, we report the synthesis of ferromagnetic $Mn_5Ge_3(Mn_5Ge_3O_y)$-$GeO_2(GeO_x)$ nanocomposite films containing ferromagnetic Mn_5Ge_3 and $Mn_5Ge_3O_y$ nanoclusters embedded into dielectric GeO_2 and GeO_x matrices via a solid state reaction between the GeO and Mn layers. A schematic illustration of the reaction in the Mn/GeO bilayer after annealing up to 300°C is presented in **Figure 1.** Annealing studies of the Mn/GeO bilayers demonstrate the start of a reduction-oxidation reaction at 180°C, producing the decomposition of GeO into Ge and germanium oxides $GeO_2(GeO_x)$, along with a solid-state reaction between the Mn and Ge that occurs simultaneously. The final reaction products at 300°C are ferromagnetic Mn_5Ge_3 and $Mn_5Ge_3O_y$ nanoclusters embedded in a $GeO_2(GeO_x)$ matrix.

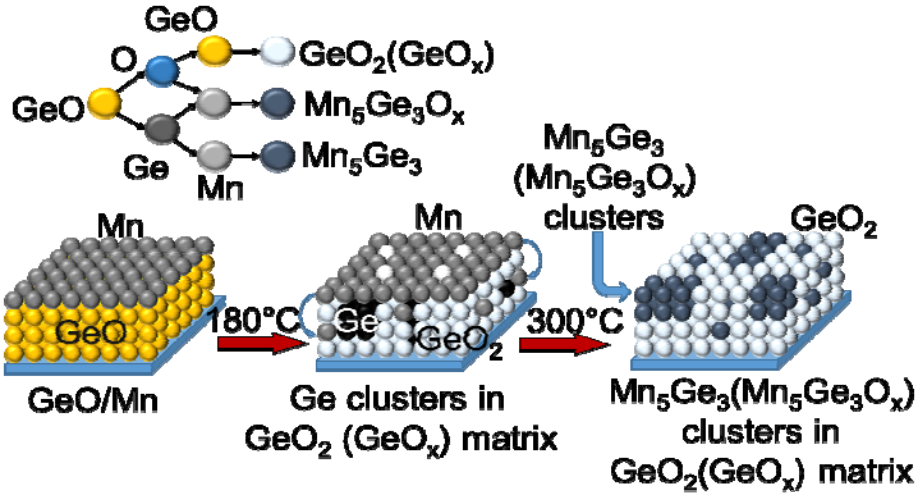

Figure 1. Solid-state synthesis of $Mn_5Ge_3(Mn_5Ge_3O_y)$-$GeO_2(GeO_x)$ nanocomposites. (a) Schematic illustration of the synthesis of ferromagnetic $Mn_5Ge_3(Mn_5Ge_3O_y)$-$GeO_2(GeO_x)$ nanostructures by annealing the A-Mn/GeO bilayers up to 300ºC. Above the initiation temperature T_{in} ~ 180°C, GeO decomposes into elemental Ge and O. Simultaneously the Ge and O atoms migrate into the Mn layer for the synthesis of the ferromagnetic $Mn_5Ge_3(Mn_5Ge_3O_y)$ nanoclusters and Ge with O forms the $GeO_2(GeO_x)$ matrix.

2. Experimental details

2.1 Sample preparation. The initial Mn/GeO films were obtained by the successive thermal deposition of the GeO and Mn layers onto chemically pure glass substrates having a thickness of 0.18 mm in a vacuum at a residual pressure of 10^{-6} Torr. Previously, the substrates were degassed at 350°C for 1 h, which was followed by the deposition of the GeO layers at a temperature of 180°C. The X-ray photoelectron spectroscopy (XPS) studies shows the formation of highly stoichiometric GeO films by the thermal deposition method. The top Mn layer was deposited at room temperature to prevent a reaction between the Mn and GeO during the deposition. The nominal thicknesses for cross-sectional TEM and resistivity were Mn(100nm), GeO(300nm) bilayers (A-Mn/GeO further in the text). The Mn(50nm)/GeO(100nm) bilayers and Mn(20nm)/GeO(30nm) films on NaCl(001) were prepared for magnetic and transmission electron microscopy (TEM) studies (B-Mn/GeO further in the text), respectively. Film thicknesses were determined by X-ray fluorescent analysis or cross-sectional TEM image. The TEM studies show the differences in structural changes between A-Mn/GeO and B-Mn/GeO during annealing up 300°C.

2.2 Synthesis. The initial Mn/GeO bilayers were annealed at temperatures between 50-500°C at 50°C intervals. The samples were held at each temperature at a pressure of 10^{-6} Torr for 1hour.

2.3 TEM characterization. The cross-sectional samples for investigation by transmission electron microscopy (TEM) were prepared using a focused ion beam (FIB, Hitachi FB2100) at 40 kV. During sample preparation a W layer was deposited in the FIB by dissolution of the $W(CO)_6$ gas in order to protect the surface of interest from milling by the Ga+ ion beam. TEM investigations were carried out using a Hitachi HT7700 TEM at 100kV (W source) equipped with a scanning TEM system and a Bruker Nano XFlash 6T/60 energy dispersive X-ray (EDX) spectrometer. The obtained Mn/GeO and GeO films were separated from the substrate, placed on a molybdenum TEM grid and annealed at 300°C for 1 h.

2.4 XPS studies. X-ray photoelectron spectra were collected using a SPECS instrument (Germany) equipped with a PHOIBOS 150 MCD 9 hemispherical analyzer at a pass energy of 20 eV for survey spectra and 8 eV for narrow scans. The Mg Kα line (1253.6 eV) of a dual anode X-ray source was used for excitation. Sample etching with Ar^+ ions was performed with a PU-IQE 12/38 scanning source operated at an accelerating voltage of 5 kV and ion emission current of 15 μA, which corresponds to a scattering rate of ~1 nm/min. Surface concentrations of elements were determined from the survey spectra using the empirical relative sensitivity factors embedded in the CasaXPS program. The high-resolution spectra were fitted with Gaussian-Lorentzian peak profiles after Shirley background subtraction.

2.5 Magnetic and resistivity measurements. Saturation magnetization M_S and Curie temperature T_C measurements were performed on a vibration magnetometer with in-plane magnetic fields up to 2 kOe. We also measured the saturation magnetization M_S and the perpendicular anisotropy constant $K_\perp = 2\pi M_S^2 \pm \Delta K_\perp$ using a torque magnetometer with a sensitivity of $3.76 \cdot 10^{-9}$ Nm in the applied field range of 0 to18 kOe at room temperature. The value of $\Delta K_\perp$ in thin films was associated with the presence of in-plane strains and grain growth textures [22, 23].

3. Results

3.1. Solid state reactions in Mn/GeO bilayers.

3.1.1. X-ray diffraction studies

Figure 2 shows the saturation magnetization $M_S(T_S)$ **(a)** and electrical resistance $R(T_S)$ **(b)** of the A-Mn/GeO bilayers as a function of annealing temperature T_S. Up to ~ 180° C, the Mn/GeO samples remained nonmagnetic, which implies the absence of mixing and the formation of magnetic phases on the Mn/GeO interface **(Figure. 2a)**. With an increase in the annealing temperature above ~ 180°C, the saturation magnetization M_S appears in the Mn/GeO films and reaches a maximum value after annealing at 300° C. This clearly indicates the onset of a solid-state reaction above the initiation temperature T_{in} ~ 180°C between the Mn and GeO layers and the synthesis of one or more ferromagnetic phases. The volume fraction of these phases in the reaction products increases up to 300°C. After annealing above 300°C, the degradation of the ferromagnetic phases reduced the magnetization, which dropped to zero at 400°C **(Figure. 2a)**. **Figure 2b** shows the temperature dependence of the electrical resistance R (T_S) of the Mn/GeO film sample, which was heated at a rate of 4°C/min to 500°C and cooled to room temperature. The slow increasing of electrical resistance $R(T_S)$ above T_{in} ~ 180°C is consistent with the start of the solid phase reaction between the Mn and GeO layers, which finished at 300°C. After annealing at 350°C the resistance $R(T_S)$ slowly decreased during cooling down to room temperature. The insignificant increasing of the

resistance (about 2.5 times) and the metallic-like temperature dependence of $R(T_S)$ explicitly indicates that after annealing at 350°C the A-Mn/GeO samples contains a residual Mn layer **(insert in Figure 2)**. The strong growth of electrical resistance $R(T_S)$ above 350°C is undoubtedly associated with the formation of a nonconducting matrix. At decreasing temperature from 500°C to room temperature the resistance $R(T_S)$ increases, which is a typical feature of semiconductor samples (**Figure 2b**).

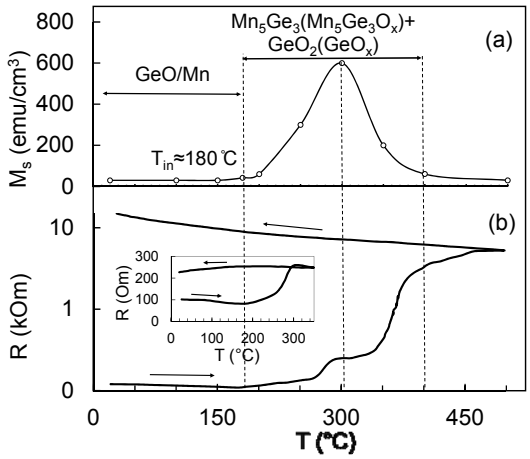

Figure 2. Determination of the initiation temperature T_{in} ~ 180 ° C of the reaction between the Mn and GeO layers. (a) The magnetization saturation M_S of the A-Mn/GeO bilayers as a function of annealing temperature T_S. The synthesis of the ferromagnetic $Mn_5Ge_3(Mn_5Ge_3O_v)$ nanoclusters in the Mn/GeO bilayers starts at T_{in} ~ 180°C and above 300°C the Mn oxidation inhibits the magnetism in the sample. **(b)** Electrical resistance of the A-Mn/GeO bilayers heated up to 500°C and cooling to room temperature as a function of the temperature measurement T_S. The inset shows the $R(T_S)$ of the Mn/GeO bilayers heated up to 300°C and then cooled to room temperature. The metallic resistance is a consequence of the unreacted Mn layer on the top of the sample.

The diffraction pattern of the starting Mn/GeO bilayers contained reflections from the Mn layer and did not change up to the initiation temperature T_{in} ~ 180°C (**Figure 3a**). The absence of reflections from the GeO layer suggests amorphous or nanocrystalline growth. After annealing at 250° C, reflections from the pure Mn decreased and reflections from the ferromagnetic Mn_5Ge_3 phase appear **(Figure 3b).** The intensity of the Mn_5Ge_3 reflections increased up to 300° C **(Figure 3c),** began to reduce above 300°C and vanished completely after annealing above 400°C (**Figure 3d).** The formation of the ferromagnetic Mn_5Ge_3 phase matches well with the occurrence of magnetization in the 180°C - 300°C temperature interval and disappears after annealing at 400°C **(Figure 2a)**. The findings suggest that a disproportionation reaction (1), producing Ge nanoclusters embedded into a GeO_2 matrix and a solid-state reaction between Ge and Mn (2) simultaneously start in the Mn/GeO interface above 180°C and completely finish after annealing at 300°C.

$$2GeO \rightarrow 2Ge^0 + GeO_2 \quad (1)$$

$$3Ge^0 + 5Mn \rightarrow Mn_5Ge_3 \quad (2)$$

The disproportionation reaction (1) of GeO_x into elemental Ge^0 and GeO_2 composite obtained by vacuum annealing is commonly used in Ge nanostructure synthesis [24-25]. Above 300°C new peaks of Ge and MnO appeared in addition to the Mn_5Ge_3 reflections and became dominant peaks above 400°C (**Figure 3d, 3e**). This suggests the structural degradation of ferromagnetic Mn_5Ge_3 by oxidation of Mn above 300°C and as a result the phase separation of Mn_5Ge_3 into elemental Ge^0 and MnO nanoclusters.

Thus, magnetic, resistance and X-ray studies designated two temperature features: the initiation temperature of the reaction between Mn and GeO is T_{in} ~ 180°C and the oxidation

of Mn in Mn_5Ge_3 nanoclusters, which is contained in the reaction products, occurs in the 300 - 500°C temperature interval.

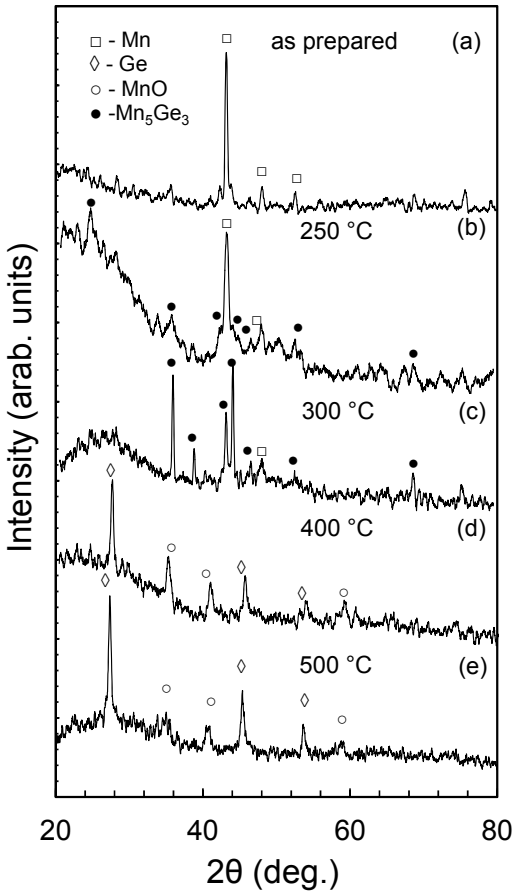

Figure 3. Structural characterization of the A-Mn/GeO bilayers. X-ray diffraction patterns of the as-deposited A-Mn/GeO bilayers (a) and after annealing at 250°C (b), 300°C (c), 400°C (d), 500°C (e).

3.1.2. Magnetization studies

In order to characterize the magnetic properties of Mn/GeO samples after annealing at 250°C and 300°C the temperature dependences of the saturation magnetization M_S **(Figure 4a)** and hysteresis loops **(Figure 4b)** of B-Mn/GeO films were measured. Both dependences indicate the formation of the Mn_5Ge_3 phase with a Curie temperature $T_C^1 \sim 300K$ [14 - 16] and a second ferromagnetic phase with $T_C^2 \sim 360 - 400K$. Recently, we reported that in the 250°C - 300°C temperature interval the migration of C and O impurity atoms into the octahedral interstitial sites of the Mn_5Ge_3 lattice leads to the formation of the Nowotny phase $Mn_5Ge_3C_xO_y$, with a Curie temperature $T_C \sim 350 - 400K$ when annealing Mn/Ge bilayers [14,15] and Ge/Ag/Mn trilayers [16]. However, EDS analysis (**Table 1**) shows a preferential presence of oxygen, which indicates that Mn_5Ge_3 and Nowotny $Mn_5Ge_3O_y$ are the main phases formed in the Mn/GeO bilayers after annealing up to 300°C. After annealing at 300°C the magnetization increased relative to annealing at 250°C due to the increase of the volume fraction of the Mn_5Ge_3 and $Mn_5Ge_3O_y$ nanoclusters in the sample. This is in good agreement with X-ray studies which show an increase in the intensity of the Mn_5Ge_3 reflections after annealing at 300 °C **(Figure 3b, 3c)**. Hysteresis loops after annealing at both 250°C and 300°C possess the ratio $M_r/M_S = 0.55$ (where M_r is magnetic remanence) similar to the Stoner–Wolfarth curve with

M_r/M_S = 0.5, which describes a random assembly of noninteracting single-domain ferromagnetic particles with uniaxial anisotropy [27]. It is known that for Mn_5Ge_3 the magnetocrystalline anisotropy constant $K_1 = 3.0\times10^5$ erg/cm^3 [28] and the exchange stiffness parameter $A_{ex}= 1 \times 10^{-7}$ erg/cm [29], and therefore the exchange length $L_{ex} = (A_{ex}/K_1)^{1/2}$ is ~ 6 nm. From this it follows that for the majority of noninteracting $Mn_5Ge_3(Mn_5Ge_3O_y)$ nanoclusters the intercluster distances must be more than 6 nm. This result agrees well with the TEM observations that are presented in **Figure 6**. The measurements of the perpendicular anisotropy constant $K\perp = 2\pi M_S^2 \pm \Delta K\perp$ using a torque method show that $\Delta K\perp \sim 0$, which indicates the lack of in-plane strains and a grain growth texture in the $Mn_5Ge_3(Mn_5Ge_3O_y)$ nanoclusters.

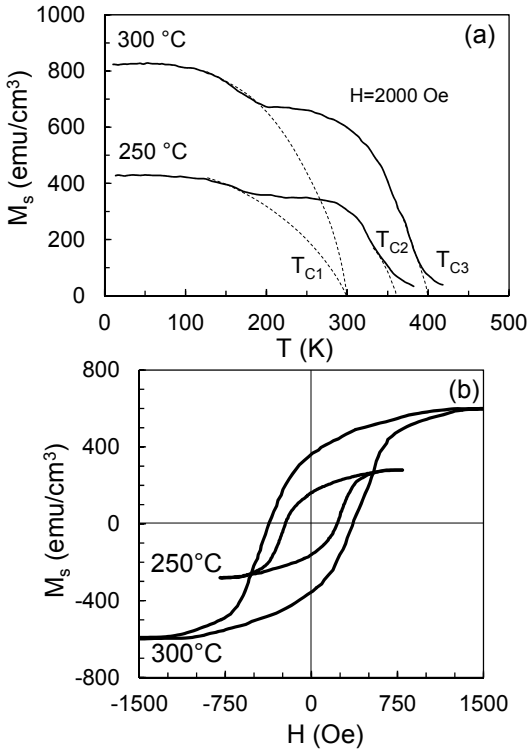

Figure 4. Temperature dependence of the saturation magnetizations of $Mn_5Ge_3(Mn_5Ge_3O_y)$-$GeO_2(GeO_x)$ nanocomposite films. Temperature dependences of the saturation magnetization M_S measured for the B-Mn/GeO bilayer after annealing at 250°C, **(a)** and 300°C, **(b)** have clearly demonstrated the existence of the Mn_5Ge_3 (T_C ~ 300K) and Nowotny $Mn_5Ge_3O_y$ (T_C ~ 350 – 400K) ferromagnetic phases. Both hysteresis loops **(b)** are consistent with the Stoner-Wohlfarth model, where the $Mn_5Ge_3(Mn_5Ge_3O_y)$ are a set of randomly oriented noninteracting nanoclusters.

Thus, magnetic studies of the B-Mn/GeO samples suggest that the final products of reactions (1), (2) contain noninteracting $Mn_5Ge_3(Mn_5Ge_3O_y)$ nanoclusters embedded into a germanium oxide matrix.

3.1.2. Cross section studies

Cross-sectional studies were performed in order to better understand the origin of the formation of ferromagnetic Mn_5Ge_3 (Mn_5Ge_3Oy)-GeO_2(GeOx) nanocomposites in the A-Mn/GeO bilayer during annealing up to 500°C. **Figure 5** shows the cross-sectional TEM images for the initial Mn(50nm)/GeO (300nm) bilayer (a) and after annealing at 200°C **(b),** and 300°C **(c).**

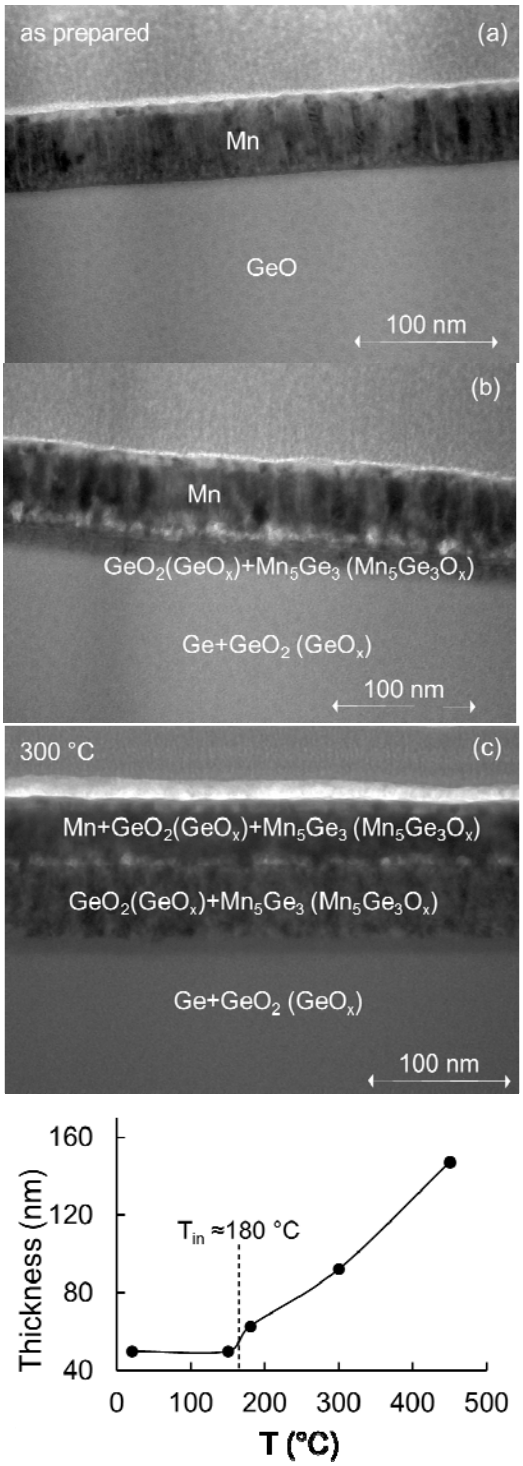

Figure 5. A direct evidence of the low-temperature synthesis of $Mn_5Ge_3(Mn_5Ge_3O_y)$-$GeO_2(GeO_x)$ in A-Mn/GeO bilayers. TEM image of the cross-section of the A-Mn/GeO bilayers: (**a**) as-deposited, (**b**) after annealing at 200ºC and (**c**) 300ºC. After annealing above 180ºC the GeO undergoes disproportion and $Mn_5Ge_3(Mn_5Ge_3O_y)$-$GeO_2(GeO_x)$ nanostructures are formed at the Mn/GeO interface. The EDS element mapping of the Mn, O and Ge in layers of the as-deposited and after annealing at 200ºC and 300ºC samples are presented in Table 1. **(d)**The thickness of the reaction product layer as a function of the annealing temperature up to 500ºC.

Table 1. The EDS element mapping of the Mn, O and Ge of the as-deposited **(a)** and after annealing at 200ºC **(b)** and 300ºC **(c)** A-Mn/GeO bilayers.

№	Layer	Chemical elements (at.%)		
		Mn	Ge	O
(a)	Mn	99	0	1
	GeO	0	50	50
(b)	Mn	98	0	2
	$GeO_2(GeO_x)$+ Mn_5Ge_3 ($Mn_5Ge_3O_x$)	60	42	8
	Ge+$GeO_2(GeO_x)$	0	50	50
(c)	Mn+$GeO_2(GeO_x)$+ Mn_5Ge_3 ($Mn_5Ge_3O_x$)	60	35	5
	$GeO_2(GeO_x)$+ Mn_5Ge_3 ($Mn_5Ge_3O_x$)	30	60	10
	Ge+$GeO_2(GeO_x)$	0	50	50

The initial Mn/GeO bilayer structure is clearly illustrated by TEM **(Figure 5a).** EDX results reveal a homogeneous distribution of Mn and Ge in the Mn (50nm) and GeO (300nm) layers, respectively, (these results are not given) and this is consistent with XRD data **(Figure 3a).** However, after annealing up to 500°C the EDX elemental mapping reveals the inhomogeneous Mn, Ge and O distribution along perpendicular directions of the Mn/GeO interface. After annealing at 200°C **(Figure 5b)** and 300°C **(Figure 5c)** the cross-sectional TEM images were conditionally divided in to three layers and in Table 1 the average distributions of Mn, Ge and O are given. The analysis of the Mn, Ge and O distributions **(Table 1)** does not show a Mn migration into the GeO layer but instead suggests a Ge migration into the Mn layer. The TEM image of the Mn(50nm)/GeO(300nm) film after annealing at 300°C **(Figure 5c)** reliably demonstrates the doubling of the Mn-based layer thickness due to the migration of a considerable quantity of Ge atoms which arises due to reaction (1) in the Mn layer. This finding agrees well with our previous studies and suggests that Ge is the dominant diffusing species in the Mn_5Ge_3 synthesis [16]. An increase in the annealing temperature up to 500°C leads to the oxidation of the Mn_5Ge_3 and Nowotny Mn_5Ge_3Oy nanoclusters and further increases in the Mn-based layer as shown in **Figure 5d**. The cross section results affirm the XRD and magnetic data that the formation of the ferromagnetic Mn_5Ge_3 and Nowotny Mn_5Ge_3Oy phases in the reaction products occurs after annealing at 300°C.

The results of the cross section studies complete the XRD and magnetic data and suggest that the reaction in Mn/GeO starts with the disproportionation reaction (1), producing elementary Ge^0, which migrates into the Mn layer and forms the ferromagnetic Mn_5Ge_3 and Nowotny $Mn_5Ge_3O_y$ nanoclusters. Above 300°C, as a result of the oxidative activity of manganese, Mn_5Ge_3 and $Mn_5Ge_3O_y$ decompose into a mixture of semiconductor Ge^0 and dielectric MnO components.

3.1.2. TEM characterizations.

The Mn(20nm)/GeO(30nm) films were used to obtain further insight about the structural differences in the formation of Mn_5Ge_3 nanoclusters in A-Mn/GeO and B-Mn/GeO samples during annealing up to 300°C. **Figure 6** shows a typical TEM image **(a)** and the selected area electron diffraction pattern (SAED) **(b)** after annealing at 300°C. The average atomic number for the GeO_x and GeO_2 phases is lower than the atomic number of Mn, thus the GeO and GeO_2 region appears brighter than the Mn region on the TEM image (**Figure 6a)**. The mapping for Ge and O is quite homogeneous in the study area, while the mapping of Mn

reveals an increased concentration of Mn in the nanoparticles. This indicates the creation of nanocomposites in the B-Mn/GeO samples that consist of $Mn_5Ge_3(Mn_5Ge_3O_y)$ nanoparticles embedded into the $GeO_2(GeO_x)$ matrix. Based on these findings, *we* suppose that the interface layer in the A-Mn/GeO samples **(Figure.4c)** is the same as the B-Mn/GeO layers contained in the $Mn_5Ge_3(Mn_5Ge_3O_y)$ nanoparticles in the $GeO_2(GeO_x)$ matrix.

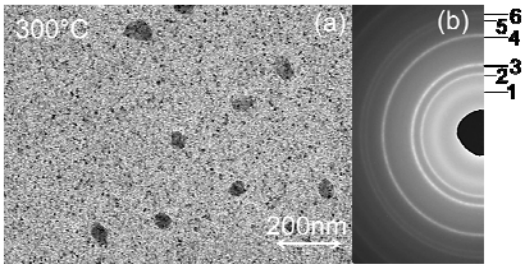

Figure 6. (a) TEM image and (b) SAED pattern of the Mn_5Ge_3 (Mn_5Ge_3Oy)-GeO_2(GeOx) film after annealing at 300°C. The sample consists of Mn_5Ge_3 (Mn_5Ge_3Oy) nanocrystals with an out-of-round morphology and nanocluster sizes of 40–80 nm separated by distances of 120-280 nm. However, Ge nanocrystals less than 20 nm are not identified by TEM and they can be present in the sample. Table 2. Indexing the diffraction reflections in (5b).

The TEM observations **(Figure 6a)** indicate that the $Mn_5Ge_3(Mn_5Ge_3O_y)$ nanoparticles have an out-of-round shape with a grain size of 50-80 nm, intercluster distances of 150-300 nm and good uniformity in the reaction product. This diameter agrees with the average size of the Mn_5Ge_3 grains determined by XRD. It is important to note that constituent part $Mn_5Ge_3(Mn_5Ge_3O_y)$ nanoparticles have sizes below 20 nm, which are not observed in the TEM image. The d-spacing obtained from the SAED pattern **(Figure 6b)** indicates the possible presence of the MnO phase besides the expected Mn_5Ge_3, $Mn_5Ge_3O_y$phases, as illustrated in Table II. The TEM results are in good agreement with magnetic studies which affirm that B-Mn/GeO samples are $Mn_5Ge_3(Mn_5Ge_3O_y)$-$GeO_2(GeO_x)$ composites containing noninteracting $Mn_5Ge_3(Mn_5Ge_3O_y)$ nanoclusters separated by distances more than 6 nm. The TEM studies show the formation of $Mn_5Ge_3(Mn_5Ge_3O_y)$-$GeO_2(GeO_x)$ films, from which it follows that an easy way to fabricate $Mn_5Ge_3(Mn_5Ge_3O_y)$-$GeO_2(GeO_x)$ nanocomposite films of different thicknesses is by annealing $(B\text{-}Mn/GeO)_n$ multilayers at 300°C.

3.2. Structural evolution of GeO films upon thermal annealing

3.2.1. Thermal annealing effect on optical properties of GeO thin films

To understand the reaction mechanism between Mn and GeO the decomposition of amorphous GeO into Ge and GeO_2 according to reaction (1) was investigated by annealing up to 500°C, and the schematic illustration is presented in **Figure 7a. Figure 7b** shows the optical density of as-deposited GeO, GeO after annealing at 300°C and Ge films having a corresponding thickness excluding the contribution of a glass substrate. The optical density at wavelengths ranging from 300 to 900 nm of the as-deposited GeO and GeO after annealing at 300°C almost coincide. The minor difference between them is the result of the presence of GeO_2 in the annealed sample. The dependence of the optical density at 400 nm of as-deposited GeO film as a function of annealing temperature is presented in **Figure 7c.** Optical density of GeO film does not change up to ~ 180°C, which evidences the lack of phase transformations in GeO film. The strong increase in the optical density above 180°C clearly demonstrates the onset of the disproportionation reaction (1) with the initiation temperature T_{in} = 180°C. The highest amount of released elemental Ge^0 in the annealed (Ge^0+GeO_2) sample is reached at a temperature of 300°C; this is evident from the maximization of the optical density at a wavelength of 400 nm **(Figure. 7c)**. As can be seen from **Figure 7c**,

further increases in the annealing temperature above 300°C leads to a decrease of the optical density which approaches zero at 500°C. This indicates the complete oxidation of germanium at 500°C and the formation of GeO_2, which has a high transparency in the visible range. Our findings are in good agreement with previously published results of the formation of Ge nanoclusters in GeO film by annealing [30-35] and an important contribution is the detection of the low initiation temperature T_{in} = 180°C of reaction (1).

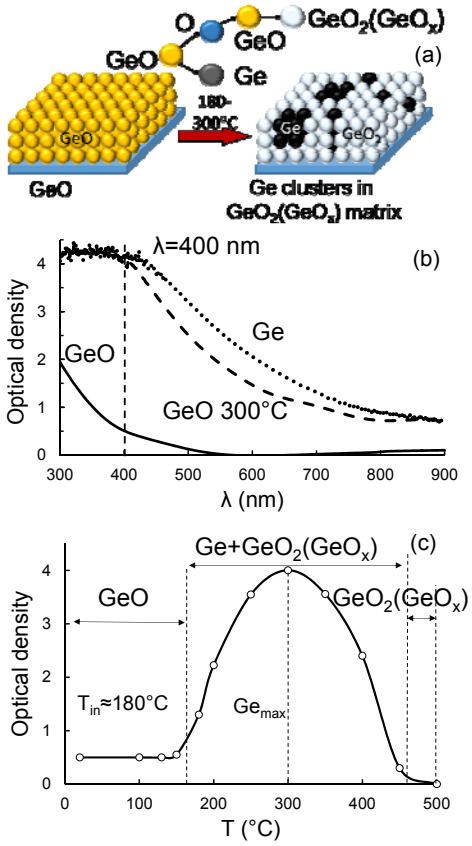

Figure 7. (a) Schematic illustration of the disproportional reaction (1), including the start at 180°C and the increase up to 300°C in the volume fraction of the Ge nanoclusters embedded in the Ge oxide matrix. **(b)** Comparison of optical spectra of as-deposited GeO film (solid), GeO after annealing at 300°C (dashed line) and Ge film having a corresponding thickness (dotted line); contribution of glass substrate is extracted from all spectra. The optical densities of Ge and GeO after annealing at 300°C coincide at 400 nm, therefore this wavelength was used for finding the dependence given in **(c). (c)**The dependence of the optical density at 400 nm of as-deposited GeO film as a function of annealing temperature. The maximal increase of the optical density at 300°C means a maximal content of Ge nanoclusters in the sample, and a strong decrease of optical density above 400°Cmeans the oxidation of Ge to GeO_2.

3.2.2. XPS of as-deposited of GeO and after annealing at 300°C

Figure 8a shows the photoelectron Ge 3d spectra of as-deposited GeO film (1, 2) and that after annealing at 300ºC (3, 4) collected before (1, 3) and after etching with Ar^+ ions to remove an oxidized surface layer (2, 4). The binding energy of 31 eV for the main peak, along with the atomic ratio O/Ge slightly above 1, indicate that a nearly stoichiometric GeO oxide was fabricated in the as-deposited sample underneath the surface of the GeO_2 (**Figure 8b)** [36]. The spectrum from the sample annealed at 300ºC (**Figure 8a**) contained

contributions with binding energies of 32.6 eV, 30.7 eV, and 29.5 eV, which can be attributed to GeO_2, GeO [38], and metallic Ge^0, respectively [37, 38]. This corroborates with the disproportionation of GeO via reaction (1). For both samples, the Ar^+ etching causes the atomic O/Ge ratio reduction to about 1 and some shifts of the GeO (Ge^{2+}) peaks due to an additional decomposition of GeO (**Figure 8a**). Similar trends can be also monitored in O 1s spectra (Supplementary Figures).

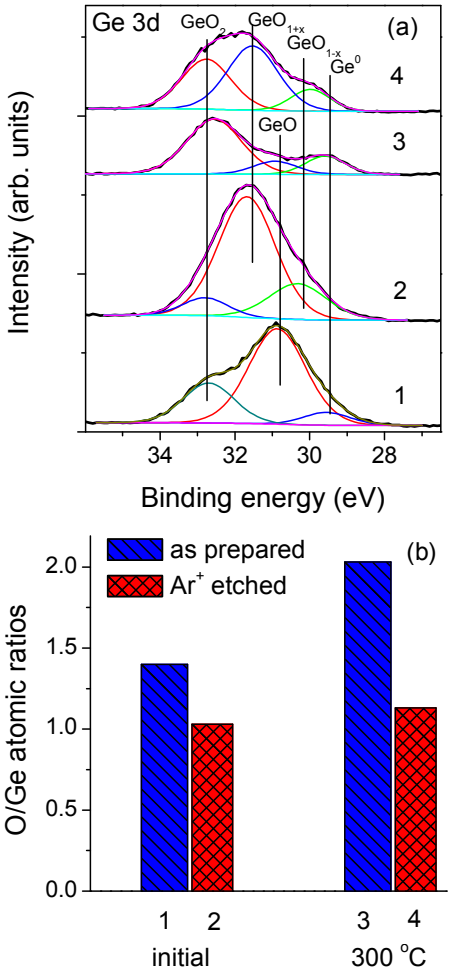

Figure 8. (a) X-ray photoelectron Ge 3d spectra of as-prepared GeO film (1,2) and the nanocomposite Ge-GeO_2(GeO_x) film annealed at 300°C (3,4). (**b**) Relative concentrations of Ge and O derived from the XPS; the data suggest that the reaction products also contain substoichiometric GeO_x in addition to GeO, GeO_2 and Ge.

Thus, the XPS findings agree with the assumption that the as-deposited films were composed of GeO oxide, which disproportionates above 180ºC, and the reaction products were Ge nanoclusters embedded into a GeO_2(GeO_x) matrix.

3.2.3. TEM images.

Figure 9 shows a typical TEM image of the as-deposited GeO film and after annealing at 300°C. The initial GeO films possessed a sand-like microstructure, which indicates that the size of the GeO nanograins is very low (< 5nm) (**Figure 9a**). The average atomic numbers for the GeO_2 and GeO_x phases are lower than the atomic number of Ge, thus the GeO_2 and GeO_x region appears brighter than the Ge region on the TEM image (**Figure 9b)** and EDS analysis confirms that the observed nanoparticles are germanium rich. After annealing at 300°C the TEM image clearly shows the formation of Ge nanoparticles of out-of-round shape with an

average grain size of ~ 60 nm and these findings are in good agreement with previously published results [34, 35]. It is important to note that the constituent part of Ge nanoparticles has a size below 20 nm, which is not observed in the TEM image. **Figure 9c** shows the SAED pattern of the GeO film after annealing at 300°C which exhibited faint diffraction rings corresponding to d-spacing of 3.25 Å, 2.0 Å 1.7 Å and 1.3 Å, which represent diffraction from the (111), (220), (311), (331) plains of Ge and there are no reflections from either GeO_2 or GeO_x. This clearly confirm the synthesis of polycrystalline Ge nanocrystals in an amorphous $GeO_2(GeO_x)$ matrix.

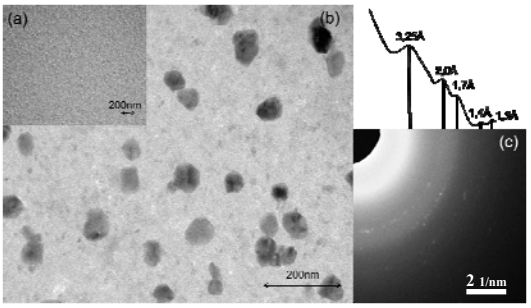

Figure 9. (a) TEM image of as-deposited GeO film, **(b)** TEM image and **(c)** the corresponding SAED pattern of the GeO film after annealing at 300°C. The TEM and SAED data confirms the presence of Ge nanocrystals in the uniform amorphous $GeO_2(GeO_x)$ matrix established on the basis of EDS and XPS analysis.

Thus, the XPS and TEM observations indicate that the as-deposited films were stoichiometric GeO oxides, which undergo the disproportionation reaction (1) above the initiation temperature ~180ºC, and after annealing at 300ºC the reaction products were Ge nanoclusters with an average diameter ~ 60 nm embedded into a $GeO_2(GeO_x)$ matrix.

4. Discussion

As is known, thin-film solid-state reactions start when the temperature of a sample T_S exceeds the initiation (formation) temperature $T_{in}(T_S>T_{in})$. For metallic thin-film reactions the initiation temperature T_{in} can be below room temperature or even below 90 K [39, 16]. Recently we showed that the initiation temperature of the Mn_5Ge_3 compound is equal to $T_{in}(Mn_5Ge_3)$ ~ 120°C [14-16] and the Ge is the sole diffusing species [16]. As pointed out above the reaction between the Mn and GeO layers starts at T_{in}(Mn/GeO) = 180°C which coincides with the initiation temperature $T_{in}(GeO \rightarrow Ge+GeO_2)$ = 180°C of the disproportionation reaction (1) that produces Ge and GeO_2, which exceeds the initiation temperature of Mn_5Ge_3 (T_{in} ~ 120°C). This result and the analysis of magnetic and structural data propose the hypothesized scenario for the synthesis of $Mn_5Ge_3 – GeO_2$ nanocomposite films. As the annealing temperature in the (Mn/GeO) bilayer increases above 180°C the GeO decomposes into elemental germanium and oxygen atoms due to reaction (1). At the same time strong chemical interactions arise between the Mn and Ge atoms and, because Ge is the sole diffusing species, the Ge atoms migrate directly into the Mn layer for the formation of the Mn_5Ge_3 nanoclusters. The oxygen released during reaction (1) not only participates in the synthesis of the Ge oxides (GeO_x, GeO_2), but also migrates into the Mn_5Ge_3 lattice and forms Nowotny $Mn_5Ge_3O_y$ nanoclusters. Above 300°C Mn is oxidized and forms a stable MnO oxide. As a consequence of this theMn_5Ge_3 and $Mn_5Ge_3O_y$ decomposes into elemental Ge and MnO and after annealing above 450°C the reaction products contain Ge, MnO, GeO_x and GeO_2 phases.

Our results demonstrate the important role of oxygen in the control of the magnetic properties of the Mn_5Ge_3-GeO_2 nanocomposites. These nanocomposites combine both the magnetic

properties of the Mn_5Ge_3 and $Mn_5Ge_3O_y$ nanoclusters and the dielectric characteristics of the GeO_x and GeO_2 oxides, providing a new room-temperature functional material.

4. Conclusion

To summarize, the solid-state reactions in the Mn/GeO bilayers were investigated in the temperature range from 50 to 500°C. The mixing of the Mn and GeO layers and the synthesis of the ferromagnetic Mn_5Ge_3 and $Mn_5Ge_3O_y$ phases at the Mn/GeO interface starts above the initiation temperature $T_{in} \sim 180$°C and the Mn_5Ge_3 and $Mn_5Ge_3O_y$ fraction volume increase after annealing up to 300°C. Annealing above 300°C leads to the oxidation of Mn in the Mn_5Ge_3 and $Mn_5Ge_3O_y$ nanoclusters with the formation of the MnO and elemental Ge and Ge oxides. Furthermore, the thin-film solid-state Mn/GeO reactions can be considered as a low-temperature technique to synthesize high-Curie temperature and high magnetization $Mn_5Ge_3(Mn_5Ge_3O_y)$-$GeO_2(GeO_x)$ nanocomposite films.

Acknowledgements

This study was supported by the Russian foundation for Basic research (grants #18-02-00779, #16-03-00069, #17-52-53031), by Russian foundation for basic research, government of Krasnoyarsk territory, Krasnoyarsk Region science and technology support fund to research project #16-42-243006 р_мол_а, # 18-42-243009 р_мол_а, by the council for grants of the president of Russian federation (SP-1373.2016.3). The XPS and Tem studies were carried out using the facilities of Performance service at Krasnoyarsk Scientific Center.

References

[1] R. Kalvig, E. Jedryka, P. Aleshkevych, M. Wojcik, W. Bednarski, M. Petit, L. Michez, Ferromagnetic resonance in Mn_5Ge_3 epitaxial films with weak stripe domain structure, J. Phys. D: Appl. Phys., 50 (2017) 125001-1 - 125001-9.

[2] E. Assaf, A. Portavoce, K. Hoummada, M. Bertoglio, S. Bertaina, High Curie temperature Mn_5Ge_3 thin films produced by non-diffusive reaction, Appl. Phys. Lett. 110 (2017) 072408-1 - 072408-4.

[3] T. Toliński, K. Synoradzki, Specific heat and magnetocaloric effect of the Mn_5Ge_3 ferromagnet, Intermetallics 47 (2014) 1-5.

[4] Y.K. Wakabayashi, R. Akiyama, Y. Takeda, M. Horio, G. Shibata, S. Sakamoto, Y. Ban, Y. Saitoh, H. Yamagami, A. Fujimori, M. Tanaka, S. Ohya, Origin of the large positive magnetoresistance of $Ge_{1-x}Mn_x$ granular thin films. Phys. Rev. B **95** (2017) 014417-1 -) 014417-6.

[5] C. Sürgers, G. Fischer, P. Winkel, H.v. Löhneysen, Magnetotransport in ferromagnetic Mn_5Ge_3, $Mn_5Ge_3C_{0.8}$ and $Mn_5Si_3C_{0.8}$ thin films. Phys. Rev. B 90 (2014) 104421-1 - 104421-9.

[6] R.P. Panguluri, C. Zeng, H.H. Weitering, J.M. Sullivan, S.C. Erwin, B. Nadgorny, Spin polarization and electronic structure of ferromagnetic Mn_5Ge_3 epilayers, Phys. stat. sol. (b) 242, (2005) R67-R69.

[7] Yu. S. Dedkov, M. Holder, G. Mayer, M. Fonin, and A. B. Preobrajenski, Spin-resolved photoemission of a ferromagnetic Mn_5Ge_3(0001) epilayer on Ge(111), J. Appl. Phys. 105 (2009) 073909-1 - 073909-4.

[8] V.L. Thanh, A. Spiesser, M.-T. Dau, S.F. Olive-Mendez, L.A. Michez, M. Petit, Epitaxial growth and magnetic properties of Mn_5Ge_3/Ge and $Mn_5Ge_3C_x$/Ge heterostructures for spintronic applications, Adv. Nat. Sci.: Nanosci. Nanotechnol. 4 (2013) 043002-1 - 043002-9.

[9] M. Petit, L. Michez, C.-E. Dutoit, S. Bertaina, V.O. Dolocan, V. Heresanu, M. Stoffel, V.L. Thanh, Very low-temperature epitaxial growth of Mn_5Ge_3 and $Mn_5Ge_3C_{0.2}$ films on Ge(111) using molecular beam epitaxy, Thin Solid Films 589 (2015) 427-432.

[10] A. Alvídrez-Lechuga, R. López Antón, J. Trinidad Holguín-Momaca, F. Espinosa-Magaña, S. Federico Olive-Méndez, Role of the substrate temperature on the growth of Mn_5Ge_3 thin films by co-deposition of Mn and Ge on Ge(001) substrates by magnetron sputtering, Thin Solid Films 616 (2016) 111-115.

[11] S. Yada, P.N. Hai, S. Sugahara, M. Tanaka, Structural and magnetic properties of $Ge_{1-x}Mn_x$ thin films grown on Ge (001) substrates, J. Appl. Phys. 110 (2011) 073903-1 - 073903-8.

[11] Truong, A. O. Watanabe, P.A. Mortemousque, K. Ando, T. Sato, T. Taniyama, K.M. Itoh, Interfacial spin-glass-like state in Mn_5Ge_3 single crystalline films grown on germanium substrates, Phys. Rev. B 91 (2015) 214425-1 - 214425-9.

[12] M Gajdzik, C Sürgers, M.T Kelemen, H.v Löhneysen, Strongly enhanced Curie temperature in carbon-doped Mn_5Ge_3 films, J. of Magn. Magn. Mater. 221 (2000) 248-254.

[13] A. Spiesser, I. Slipukhina, M.-T. Dau, E. Arras, V. Le Thanh, L. Michez, P. Pochet, H. Saito, S. Yuasa, M. Jamet, and J. Derrien, Control of magnetic properties of epitaxial $Mn_5Ge_3C_x$ films induced by carbon doping, Phys. Rev. B 84 (2011) 165203-1 - 165203-7.

[14] V.G. Myagkov, V.S. Zhigalov, A.A. Matsynin, L.E. Bykova, Yu.L. Mikhlin, G.N. Bondarenko, G.S. Patrin, G.Yu. Yurkin, Formation of ferromagnetic germanides by solid-state reactions in 20Ge/80Mn films, Thin Solid Films 552 (2014) 86-91.

[15] V.G. Myagkov, V.S. Zhigalov, A.A. Matsynin, L.E. Bykova, G.V. Bondarenko, G.N. Bondarenko, G.S. Patrin, D.A. Velikanov, Phase transformations in the Mn-Ge system and in Ge_xMn_{1-x} diluted semiconductors, JETP Letters, 96 (2012) 40-43.

[16] V.G. Myagkov, L.E. Bykova, A.A. Matsynin, M.N. Volochaev, V.S. Zhigalov , I.A. Tambasov, Yu.L. Mikhlin , D.A. Velikanov, G.N. Bondarenko, Solid State Synthesis of Mn_5Ge_3 in Ge/Ag/Mn trilayers: Structural and magnetic studies, J. Solid State Chem. 246 (2017) 379-387.

[17] W. Yin, C.D. Kell, L. He, M.C. Dolph, C. Duska, J. Lu, R. Hull, J.A. Floro, S.A. Wolf, Enhanced magnetic and electrical properties in amorphous Ge: Mn thin films by non-magnetic codoping, J. Appl. Phys. 111 (2012) 033916-1 - 033916-7.

[18] S. Tardif, S. Cherifi, M. Jamet, T. Devillers, A. Barski, D. Schmitz, N. Darowski, P. Thakur, J. C. Cezar, N. B. Brookes, R. Mattana, J. Cibert, Exchange bias in GeMn nanocolumns: The role of surface oxidation, Appl. Phys. Lett. 97 (2010) 062501-1-062501-3.

[19] B. Toydemir, A.C. Onel, M. Ertas, L. Colakerol Arslan, Role of nitrogen on the magnetic properties of MBE grown $Mn_{0.04}Ge_{0.96}$ films, J. Magn. Magn. Mater. 393 (2015) 220-225.

[20] P. De Padova, J.-P. Ayoub, I. Berbezier, J.-M. Mariot, A. Taleb-Ibrahimi, M.C. Richter, O. Heckmann, A.M. Testa, D. Fiorani, B. Olivieri, S. Picozzi, K. Hricovini, Mn_xGe_{1-x} thin layers studied by TEM, X-ray absorption spectroscopy and SQUID magnetometry, Surf. Sci. 601(2007) 2628-2631.

[21] A. Continenza, G. Profeta, Role of oxygen defects in diluted Mn:Ge, Phys. Rev. B 78 (2008) 085215-1 - 085215-7.

[22] K. Sato, T. Mizoguchi, Simple analysis of torque measurement of magnetic thin films, J. Appl. Phys.47 (1976) 4669 - 4671.

[23] S. Chikazumi, Epitaxial growth and magnetic properties of single-crystal films of iron, nickel, and permalloy, J. Appl. Phys. 32 (1961) 81S.

[24] K. Vijayarangamuthu, S. Ratha, D. Kabiraj, D.K. Avasthi, P.K. Kulriya, V.N. Singh, B.R. Mehta, Ge nanocrystals embedded in a GeO_x matrix formed by thermally annealing of Ge oxide films, J. Vac. Sci. Technol. A 27 (2009) 731-733.
[25] S. K. Wang, H.-G. Liu, A. Toriumi, Kinetic study of GeO disproportionation into a GeO_2/Ge system using x-ray photoelectron spectroscopy, Appl. Phys. Lett. 101, 061907 (2012) 061907-1 – 061907-4.
[26] C.J. Sahle, C. Sternemann, H. Conrad, A. Herdt, O.M. Feroughi, M. Tolan,A. Hohl, R. Wagner, D. Lützenkirchen–Hecht, R. Frahm, A. Sakko, K. Hämäläinen, Phase separation and nanocrystal formation in GeO, Appl. Phys. Lett. 95 (2009) 021910-1 – 021910-3.
[27] E.C. Stoner, E.P. Wohlfarth, A Mechanism of Magnetic Hysteresis in Heterogeneous Alloys, Philos. Trans. R. Soc. London, Ser. A. 240 (1948) 599-642.
[28] A. Spiesser, F. Virot, L.-A. Michez,, R. Hayn, S. Bertaina, L. Favre, M. Petit, V. Le Thanh, Magnetic anisotropy in epitaxial Mn_5Ge_3 films, Phys. Rev. B 86 (2012) 035211-1 - 035211-16.
[29] Y. Tawara, K. Sato, On the Magnetic Anisotropy of Single Crystal of Mn_5Ge_3, J. Phys. Soc. Jpn. 18 (1963) 773-777.
[30] K. Vijayarangamuthu, S. Rath, D. Kabiraj, D.K. Avasthi, P.K. Kulriya, V.N. Singh, B.R. Mehta, Ge nanocrystals embedded in a GeOx matrix formed by thermally annealing of Ge oxide films, J. Vac. Sci. Technol A **27** (2009) 731-733
[31] C.J. Sahle, C. Sternemann, H. Conrad, A. Herdt, O.M. Feroughi, M. Tolan, A. Hohl, R. Wagner, D. Lützenkirchen–Hecht, R. Frahm, A. Sakko, K. Hämäläinen, Phase separation and nanocrystal formation in GeO, Appl. Phys. Lett. **95** (2009) 021910-1 - 021910-3.
[32] S. Kai Wang, H.-G. Liu, A. Toriumi, Kinetic study of GeO disproportionation into a GeO_2/Ge system using x-ray photoelectron spectroscopy, Applied Physics Letters 101 (2012) 061907-1 - 061907-1.
[33] J. A. McLeod, J. Zhao, L. Yang, Y. Liu, L. Liu. (2017) Structural evolution of reduced GeO_x nanoparticles. Phys. Chem. Chem. Phys. 19 (2017) 3182-3191.
[34] Y. Barta, D. Kabiraj, D. Kanjilan, Development of Ge nanoparticles embedded in GeO_2 matrix, J. Nanosci. Nanotechnol., 8 (2008) 4081-4085.
[35] J. Wu, L. Han, N. Wang, Y. Song, H. Chen, H. Chen, J. Hu, *In situ* structural evolution from GeO nanospheres to GeO/(Ge, GeO_2) core-shell nanospheres and to Ge hollow nanospheres**,** CrystEngComm 2011 (13) 4611-4616.
[36] S.K. Wang, H.-G. Liu, A. Toriumi, Kinetic study of GeO disproportionation into a GeO_2/Ge system using x-ray photoelectron spectroscopy, Appl. Phys. Lett. **101** (2012) 061907-1 – 061907-4.
[37] N. M. Bom, G. V. Soares, S. Hartmann, A. Bordin, and C. Radtke, GeO_2/Ge structure submitted to annealing in deuterium: Incorporation pathways and associated oxide modifications, Appl. Phys. Lett. **105** (2014) 141605-1 - 141605-4.
[38] T. Sasada, Y. Nakakita, M. Takenaka, S.Takagia, Surface orientation dependence of interface properties of GeO_2/Ge metal-oxide-semiconductor structures fabricated by thermal oxidation, J. Appl. Phys., **106** (2009) 073716-1 - 073716-7.
[39] V. Myagkov, O. Bayukov, Yu. Mikhlin, V. Zhigalov, L. Bykova, G.Bondarenko Galina, Long-Range Chemical Interactions in Solid-State Reactions: Effect of an Inert Ag Interlayer on the Formation of $L1_0$-FePd in Epitaxial Pd(001)/Ag(001)/Fe(001) and Fe(001)/Ag(001)/Pd(001) Trilayers, Phil. Mag. 94 (2014) 2595-2622.

Author Contributions

V.G. and A.M. design the experiments. V.G., A.M. and L.B. wrote the manuscript. L.B. performed the electrical experiments. V.Z. and A.M., synthesized all the samples. Yu.M.

carried out XPS experiments. M.V. carried out TEM cross-sectional studies D.V. performed the magnetic experiment. A.A. carried out optical experiments. G.B. performed X-ray diffraction experiments. V.G., A.M., L.B., V.Z., Yu. M., M.V. and A.A. interpreted the data and were involved in discussions and analysis of the results. All authors contributed to the writing of the manuscript.

Additional Information

Competing Interests: The authors declare no competing financial interests.